

LAMA-Net: Unsupervised Domain Adaptation via Latent Alignment and Manifold Learning for RUL Prediction

Manu Joseph,¹ Varchita Lalwani,¹

¹ Applied Research, Thoucentric
Bangalore, India

manujoseph@thoucentric.com, varchitalalwani@thoucentric.com

Abstract

Prognostics and Health Management (PHM) is an emerging field which has received much attention from the manufacturing industry because of the benefits and efficiencies it brings to the table. And Remaining Useful Life (RUL) prediction is at the heart of any PHM system. Most recent data-driven research demand substantial volumes of labelled training data before a performant model can be trained under the supervised learning paradigm. This is where Transfer Learning (TL) and Domain Adaptation (DA) methods step in and make it possible for us to generalize a supervised model to other domains with different data distributions with no labelled data. In this paper, we propose *LAMA-Net*, an encoder-decoder based model (Transformer) with an induced bottleneck, Latent Alignment using Maximum Mean Discrepancy (MMD) and manifold learning is proposed to tackle the problem of Unsupervised Homogeneous Domain Adaptation for RUL prediction. *LAMA-Net* is validated using the C-MAPSS Turbofan Engine dataset by NASA and compared against other state-of-the-art techniques for DA. The results suggest that the proposed method offers a promising approach to perform domain adaptation in RUL prediction. We have made available the code at <https://github.com/repo>.

Introduction

Prognostics and Health Management (PHM) is an emerging field which has received much attention from the manufacturing industry because of the benefits and efficiencies it brings to the table. The amount of time a machine will probably continue to function before needing repair or replacement is known as the Remaining Useful Life (RUL). RUL prediction is at the heart of any PHM system.

The RUL prediction problem has been addressed in literature with respect to physics, statistical and machine learning methodologies. The failure mechanisms' degradation processes are described mathematically using physics-based methodologies (Cubillo, Perinpanayagam, and Esperon-Miguez (2016)). These methods demand prior knowledge of deterioration and offer precise RUL estimation when failure can be explained by its physical characteristics. Statistical techniques typically make an effort to fit the data to a probabilistic theory that can capture the uncertainty in the

deterioration process (Si et al. (2011)). Their flaws are related to data distributions and assumptions regarding changes in health state. In contrast, machine learning models concentrate on discovering the patterns of degradation directly from gathered complex raw data. Machine Learning models like Support Vector Regression (SVR) (Drucker et al. (1997)), Random Forest (Breiman (2001)), XgBoost (Chen and Guestrin (2016)), and deep learning models like LSTMs (Hochreiter and Schmidhuber (1997)) have been used for prognostic prediction challenges.

Although data-driven approaches based on deep learning have produced promising results for RUL prediction tasks, these approaches require a significant amount of labelled datasets for the network to be trained before it can provide a model that is accurate enough. However, it is frequently challenging to gather enough data with run-to-failure information for complicated systems, especially when companies already use time-based maintenance schedules. Even when we have enough run-to-failure data, models trained on one specific dataset may not generalize well even if some operating conditions change, or some new failure mode is introduced and so on. Although we can start collecting data for the new condition and retrain the models, it usually takes some time to collect the require run-to-failure data. These type of changes (data distribution changes, different input features, limited fault information) is called, collectively, *domain shift*.

In machine learning, one of the ways this shift is tackled is by using *Transfer Learning (TL)*, more specifically *Domain Adaptation (DA)*. DA is a special case of TL where the learning task remains the same, but we move from one domain to another. Several algorithms have been proposed over the years to tackle DA, mostly by reducing domain discrepancy (Gretton et al. (2012))(Tzeng et al. (2014)) between source and target or adversarial learning (Ganin et al. (2016)). But the large majority of research in the area is in adapting classification tasks with very few addressing regression. And fewer work has targets the specific problem of RUL prediction.

In this work, we propose an unsupervised, homogeneous domain adaptation model with an encoder-decoder structure which uses latent alignment and domain agnostic manifold learning for RUL prediction. Latent alignment is done using Maximum Mean Discrepancy (MMD) (Gretton et al. (2012)) and manifold learning is done using a combination of

GRU(Cho et al. (2014)) based autoencoder and smoothness constraints. We use the C-MAPSS NASA Turbofan degradation dataset (Saxena et al. (2008)) to validate our results against other state-of-the-art techniques for DA. We chose this dataset because they contain four run-to-failure data under different operating conditions and failure modes.

The main contributions of the study are:

- Designing a robust domain-agnostic manifold learning mechanism by the Squeeze Layer and GRU based autoencoder
- To the best of our knowledge, we are the first to use an autoencoder for domain adaptation for a regression problem.
- Novel application of smoothness (uniform continuity) constraints for regression tasks

The following sections of this article are organized as follows: Section 2 explains the background and related work. Section 3 describes the methodology, and Section 4 explains the experimental results and ablation analysis. Section 5 presents conclusions and future work.

Related Work

RUL Prediction approaches

The different approaches for RUL prediction can be broadly classified into - model-based (Physics based) (Cubillo, Perinpanayagam, and Esperon-Miguez (2016), data-driven (Fang et al. (2018)) and hybrid (Lei et al. (2018)). Physics-based approaches, although are high fidelity, are usually limited to a few specific components or to similar ones. Data-driven methods are more general because they don't have the strong assumptions Physics-based approaches have.

Statistical methods like survival analysis and hidden markov models have successfully been used in RUL prediction (Si et al. (2011)). Modern machine learning approaches like LGBM (Li et al. (2018a)), XgBoost (Ma et al. (2020)) and ensembles of Multi-Layered Perceptrons (Jianzhong et al. (2010)) have been used for RUL Prediction. But the recent surge of interest in deep learning has led to a lot of work in using deep learning models for RUL prediction (Wang, Zhao, and Addepalli (2020)). (Huang et al. 2007) proposed a Feed Forward Network for RUL prediction and showed that it surpassed reliability based approaches. Zheng et al. (2017) proposed a Long Short-Term Memory (LSTM) approach for RUL estimation which made full use of the sensor sequence information and exposed hidden patterns within sensor data with multiple operating conditions, fault and degradation models.(Li, Ding, and Sun (2018)) showed the effectiveness of Deep Convolutional Neural Networks (DCNN) in estimating RUL. (Peng et al. (2021a)) used an LSTM to extract the temporal characteristics of the data sequence, one-dimensional fully-convolutional layer is adopted to extract spatial features. The spatio-temporal features extracted by the two models are fused and used as the input of the one-dimensional convolutional neural network for RUL prediction. Attention-based DCNN architecture to predict the RUL of turbofan engines with feature ranking metric is explored in (Muneer et al. (2021)).

Although Transformers(Vaswani et al. (2017)) have been used for time series prediction(Wu et al. (2021), Zhou et al. (2021)), the focus was mostly on capturing the dependencies between time steps. Zhang, Song, and Li (2021) proposed a Transformer based Dual Aspect Self Attention (DAST) model which captured the dependencies between time steps as well as different sensors for RUL prediction.

Domain Adaptation for PHM

All the methods discussed above assumes that sufficient labelled training data is available and that the training and test data are drawn from the same distribution. But in many real-world problems, this is simply not the case. A subset of *Transfer Learning (TL)*, called *Domain Adaptation (DA)* has been developed to address this situation.

The conventional approach for DA re-weights the source samples by looking at the similarity with target samples(Huang et al. (2006)). Subspace Alignment methods (Fernando et al. (2013)) attempt to find a linear map between a number of top eigenvectors by minimizing the Frobenius norm between them. Other approaches attempt to reduce the domain shift problem by minimizing the divergence between source and target features. (Tzeng et al. (2014), Long et al. (2015)) used Maximum Mean Discrepancy (MMD) (Gretton et al. (2012)) in a CNN architecture with an adaptation layer to learn a representation that is both semantically meaningful and domain invariant on image dataset. CORrelation ALignment or CORAL (Sun and Saenko (2016)) is another simple yet effective method for minimizing the domain shift by aligning the second-order statistics of source and target distributions. Another approach, based on the theory by Ben-David et al. (2010), is to use a classification loss to directly confuse between domains using adversarial training (Ganin et al. (2016), (Ajakan et al. 2014)).

A large majority of research in DA has focused on image datasets and classification problems. Adapting such methods to the RUL prediction task, which has a sequential input instead of a spatial one and is a regression rather than a classification, is not trivial. Zhang et al. (2018) used a Bi-directional LSTM in a transfer learning paradigm to transfer between domains. But it still needed a few training labels on the target data. It is also worth noting that when transferring from multi-type operating conditions to single operating conditions, transfer learning led to a worse result. de Oliveira da Costa et al. (2020) has applied unsupervised Domain-Adversarial Neural Networks (DANN) for the RUL prediction domain with some success. (Li, Li, and He (2019)) focuses on a domain adaptation RUL prediction model by integrating the adaptive batch normalization (AdaBN) (Li et al. (2018b)) into DCNN. Ding, Jia, and Cao (2021) proposed Deep Subdomain Adaptive Regression Network(DSARN) which tries to make the alignment between source and target on sub-domains rather than global alignment. Ragab et al. (2021) proposed a two-step domain adaptation technique using adversarial domain adaptation and contrastive loss to generalize between target and source.

Domain Adaptation through Manifold Learning

Autoencoders have been used for manifold learning (Wei et al. (2016)) in the semi-supervised setting. They have also been used for domain adaptation (Deng et al. (2014)). The success of such approaches lies in the ability of the autoencoder to learn the underlying manifold in the input space. Many approaches also use explicit manifold geometry based alignment functions (Baktash et al. (2014), Wang et al. (2018)) to learn a domain agnostic manifold and perform domain adaptation through it. But these approaches usually introduce some computational instability and complexity.

LAMA-Net: Unsupervised Domain Adaptation via Latent Alignment and Manifold Learning

In this section, we present *LAMA-Net* (Unsupervised Domain Adaptation via Latent Alignment and **MAN**ifold Learning), our domain adaptation model to predict the RUL of assets across different domains with different fault modes and operating conditions. We will first introduce, formally, the problem definition and then go on in detail about the model architecture, the different components used, and the training and optimization.

Problem Definition

Given a source domain, \mathcal{D}_s , and a corresponding learning task, \mathcal{T}_s , a target domain, \mathcal{D}_t and a learning task, \mathcal{T}_t . For the domain adaptation setting, we have $\mathcal{T}_s = \mathcal{T}_t$ and $\mathcal{D}_s \neq \mathcal{D}_t$.

We make the following assumptions/notations:

- The source domain, $\mathcal{D}_s = \{(x_s^i, y_s^i)\}_{i=1}^{N_s}$, contain N_s training examples and $x_s^i \in \mathcal{X}_s$ is a sequence of multivariate time-series sensor data of length K_t and f features, i.e. $x_s^i \in \mathbb{R}^{f \times K_t}$. $y_s^i \in \mathcal{Y}_s$ denotes the Remaining Useful Life (RUL) for each sequence x_s^i
- The target domain, $\mathcal{D}_t = \{(x_t^i)\}_{i=1}^{N_t}$, contain N_t training examples and $x_t^i \in \mathcal{X}_t$ is a sequence like the target domain but without a target value (*unsupervised domain adaptation*)
- \mathcal{D}_s and \mathcal{D}_t are sampled from distinct marginal probability distributions $\mathbb{P}(\mathcal{X}_s) \neq \mathbb{P}(\mathcal{X}_t)$
- $x_t^i \in \mathbb{R}^{f \times K_t}$ to have the same number of features as the source domain (*homogeneous domain adaptation*), but sampled from a different probability distribution
- We denote the number of training examples for source and target separately as N_s and N_t purely for the ease of exposition. Practically, while training, $N_s = N_t$.

Our goal is to learn a function, g , which approximates the RUL in the target domain at testing time directly from degradation data, i.e. $y_t^i \approx g(x_t^i)$. We have considered the length of source sequence, K_s , and target sequence, K_t , to be same but it can be different as per domain and the proposed method would be able to handle such differences using padding.

Model Architecture

The model architecture (Figure 1) follows a Siamese-twins like parallel streams which processes source and target domain input examples. All the components in the network architecture is shared between the source and target domains with sufficient incentives for the latent representations to be domain agnostic so that we can generalize across domains. The model architecture has these main components:

- Encoder
- Squeeze and Expand Layers
- Decoder
- Latent Alignment via Maximum Mean Discrepancy Loss
- Reconstruction Loss
- Manifold Learning
- Loss Function

Encoder

The model architecture uses an encoder-decoder framework to encode the raw input signals into a latent space and then decode the latent representation into RUL prediction. We represent the *encoder* as a non-linear function, Enc , which transforms the input, $\mathcal{X} \in \mathbb{R}^{f \times K}$ to a latent representation, $\mathcal{E} \in \mathbb{R}^M$, where M is the latent dimension. Formally, for both the source and target domain, we have

$$\mathcal{E}_s = Enc(\mathcal{X}_s) \quad \mathcal{E}_t = Enc(\mathcal{X}_t) \quad (1)$$

Although *LAMA-Net* is agnostic to the kind of encoder-decoder we are using, for the purposes of this paper we have chosen a transformer based encoder-decoder model which has showed state-of-the-art performance in RUL prediction - Dual Aspect Self-Attention based on Transformer (DAST) for Remaining Useful Life Prediction (Zhang, Song, and Li (2021)). DAST model is a transformer-based model which uses self attention that captures the weighted features from both the sensor and time step dimensions. The DAST encoder consists of a sensor encoder layer, time step encoder layer, and a feature fusion layer, which combines the two generated weighted features from sensor and time step encoder layers. The DAST decoder is similar to the original Transformer (Vaswani et al. (2017)).

Squeeze and Expand Layer

Depending on the type of encoder function we use, M , the latent dimension, can be arbitrarily large or small. To be truly agnostic of the type of encoder used, we have introduced explicit *Squeeze* and *Expand* Layers to introduce a bottleneck in the information flow. This bottle neck is essential so that the alignment we want across the source and target domains can be done in a space without any noise and be more efficient because of it. The *Squeeze* and *Expand* Layers are layered feed forward networks of the form, $\sigma(\mathbb{W}x + b)$, where σ is any non-linear activation function.

Let us represent the non-linear function learned by the *Squeeze Layer* as S and the *Expand Layer* as E . The *Squeeze Layer* takes in the latent representation from the encoder, \mathcal{E} , and squeezes representation into $\mathcal{C} \in \mathbb{R}^B$, where B is

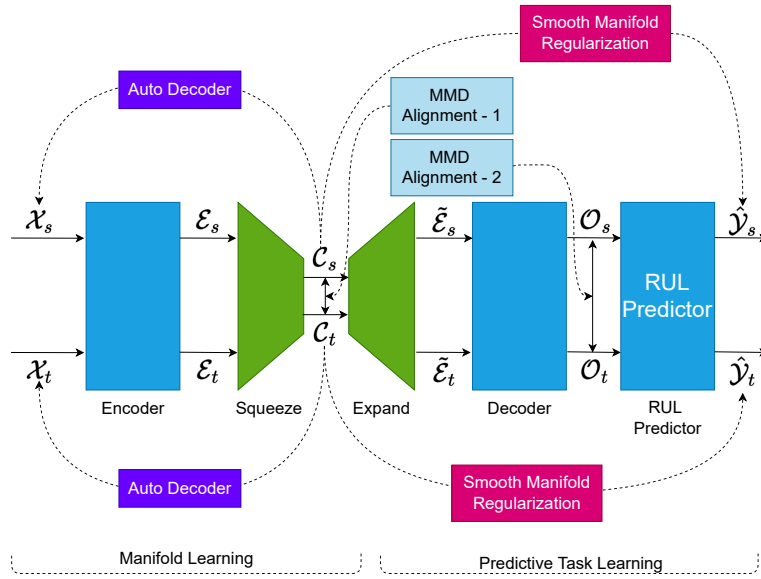


Figure 1: LAMA-Net Architecture

the bottleneck dimension and $B \ll M$. Formally, for both source and target domains, we have

$$\mathcal{C}_s = S(\mathcal{E}_s) \quad \mathcal{C}_t = S(\mathcal{E}_t) \quad (2)$$

The *Expand Layer* (E) takes in the bottleneck representation, $\mathcal{C} \in \mathbb{R}^B$, and transforms it back to the same dimension as the initial latent representation, $\tilde{\mathcal{E}} \in \mathbb{R}^M$. Formally, for both source and target domains, we have

$$\tilde{\mathcal{E}}_s = E(\mathcal{C}_s) \quad \tilde{\mathcal{E}}_t = E(\mathcal{C}_t) \quad (3)$$

Decoder and RUL Prediction

The decoder (D) takes the expanded latent representation, $\tilde{\mathcal{E}} \in \mathbb{R}^M$, and transforms into a representation suitable for the linear RUL prediction layer (R), $\mathcal{O} \in \mathbb{R}^P$, where P is the dimension of the hidden representation just before the linear RUL prediction layer. Formally, for both source and target domains, we have

$$\mathcal{O}_s = D(\tilde{\mathcal{E}}_s) \quad \mathcal{O}_t = D(\tilde{\mathcal{E}}_t) \quad (4)$$

The final linear RUL Prediction layer takes in $\mathcal{O} \in \mathbb{R}^P$ and transforms it into the final RUL Prediction, $\mathcal{Y} \in \mathbb{R}^1$, using a simple linear layer with a weight matrix, W_R , a bias matrix, b_R , and a non-linear activation function, σ . Formally, for both source and target domains, we have

$$\begin{aligned} \hat{\mathcal{Y}}_s &= R(\mathcal{O}_s) = \sigma(W_R \mathcal{O}_s + b_R) \\ \hat{\mathcal{Y}}_t &= R(\mathcal{O}_t) = \sigma(W_R \mathcal{O}_t + b_R) \end{aligned} \quad (5)$$

The $\hat{\mathcal{Y}}_s$ is compared to the actual RUL, \mathcal{Y}_s using the standard mean squared error (MSE).

$$\mathcal{L}_{RUL} = \frac{1}{N_s} \sum_{i=1}^{N_s} (y_s^i - \hat{y}_s^i)^2 \quad (6)$$

This loss (\mathcal{L}_{RUL}) ensures the network learns the right kind of representations so that the final task of predicting the RUL is learned well enough.

Latent Alignment via Maximum Mean Discrepancy

We know that \mathcal{D}_s and \mathcal{D}_t are sampled from distinct marginal probability distributions, $P(\mathcal{X}_s)$ and $P(\mathcal{X}_t)$. Because of the weight sharing in the proposed network generalization from \mathcal{D}_s to \mathcal{D}_t can happen efficiently only when the network learns domain agnostic latent representations. And to this effect, our proposed method strives to align the probability distributions of latent representations, namely \mathcal{C} and \mathcal{O} , using Maximum Mean Discrepancy (MMD).

Maximum Mean Discrepancy (MMD) is an effective non-parametric metric for measuring the discrepancy between two marginal probability distributions by embedding distributions in a reproducible kernel Hilbert space (RKHS) (Gretton et al. (2012)). Kernel embeddings of distributions allows us to embed a distribution, \mathbb{P} , into an RKHS, \mathcal{H}_ϕ , with a kernel ϕ (Sriperumbudur et al. (2010)). In the RKHS, \mathbb{P} is represented as an element, $\mu_{\mathbb{P}}$. Formally, $\mu_{\mathbb{P}} := \mathbb{E}_{x \sim \mathbb{P}} [\phi(\cdot, x)] \in \mathcal{H}_\phi$, where $x \sim \mathbb{P}$ means that random variable x has probability distribution \mathbb{P} , $\mathbb{E}_{x \sim \mathbb{P}} [f(x)]$ denotes the expectation of function f with respect to the random variable x . The kernel embedding captures all the properties about the distribution like the mean, variance, and other higher order moments if ϕ is *characteristic* (e.g. RBF Kernel) (Sriperumbudur et al. (2010)). Now we can define MMD as the RKHS norm between the kernel embeddings of two distributions.

For the source and target domains, we can formally define MMD as,

$$\begin{aligned} MMD(\mathbb{P}_s, \mathbb{P}_t) &= \|\mu_{\mathbb{P}_s} - \mu_{\mathbb{P}_t}\|_{\mathcal{H}_\phi} \\ &= \|\mathbb{E}_{x \sim \mathbb{P}_s} [\phi(\cdot, x)] - \mathbb{E}_{y \sim \mathbb{P}_t} [\phi(\cdot, y)]\|_{\mathcal{H}_\phi} \end{aligned} \quad (7)$$

We have $MMD(\mathbb{P}_s, \mathbb{P}_t) = 0$ iff $\mathbb{P}_s = \mathbb{P}_t$. If we denote $\mathcal{C}_s = \{x_s^i\}_{i=1}^{N_s}$ and $\mathcal{C}_t = \{x_t^i\}_{i=1}^{N_t}$ as two sets of samples drawn *i.i.d* from distributions s and t respectively, the empirical estimate of MMD can be given by (Gretton et al. (2012)),

$$MMD^2(\mathcal{C}_s, \mathcal{C}_t) = \left\| \frac{1}{N_s} \sum_{i=1}^{N_s} \phi(x_s^i) - \frac{1}{N_t} \sum_{i=1}^{N_t} \phi(x_t^i) \right\|_{\mathcal{H}_\phi}^2 \quad (8)$$

We can cast Eq.8 into a vector-matrix multiplication form and come up with the *kernelized* equation (Borgwardt et al. (2006))

$$MMD^2(\mathcal{C}_s, \mathcal{C}_t) = \left(\frac{1}{N_s^2} \sum_{i=1}^{N_s} \sum_{j=1}^{N_s} \phi(x_s^i, x_s^j) + \frac{1}{N_t^2} \sum_{i=1}^{N_t} \sum_{j=1}^{N_t} \phi(x_t^i, x_t^j) - \frac{2}{N_s N_t} \sum_{i=1}^{N_s} \sum_{j=1}^{N_t} \phi(x_s^i, x_t^j) \right) \quad (9)$$

We use MMD to align the feature distribution of two latent representations, \mathcal{C}_s and \mathcal{C}_t as well as \mathcal{O}_s and \mathcal{O}_t to make the learned latent representations domain agnostic. Formally,

$$\mathcal{L}_{MMD} = MMD(\mathcal{C}_s, \mathcal{C}_t) + MMD(\mathcal{O}_s, \mathcal{O}_t) \quad (10)$$

Reconstruction Loss

To induce more structure into the compressed latent representation, \mathcal{C} , we propose to add a reconstruction loss (\mathcal{L}_{recon}) which uses a standard GRU(Cho et al. (2014)) based decoder to reconstruct the input, \mathcal{X} . We construct the initial hidden state of the GRU from the compressed latent, \mathcal{C} using a simple linear layer. Formally, we can represent this as

$$h_s = \sigma(W_r \mathcal{C}_s + b_r) \quad h_t = \sigma(W_r \mathcal{C}_t + b_r) \quad (11)$$

Without going into details of the gating mechanism, the learned function by the GRU can be represented as,

$$\hat{x}_s = g(h_s; \theta_r) \quad \hat{x}_t = g(h_t; \theta_r) \quad (12)$$

We use the first element in the sequence and the hidden state constructed from \mathcal{C} to reconstruct the input sequence. The reconstruction loss (\mathcal{L}_{recon}) is the standard MSE loss and is represented formally as

$$\mathcal{L}_{recon} = \frac{1}{N_s} \sum_{i=1}^{N_s} (x_s^i - \hat{x}_s^i)^2 + \frac{1}{N_t} \sum_{i=1}^{N_t} (x_t^i - \hat{x}_t^i)^2 \quad (13)$$

Manifold Learning and Smoothness Constraint

The manifold hypothesis states that many high-dimensional datasets from the real world, actually lie along a low-dimensional manifold embedding inside that high-dimensional space (Cayton (2005)). We hypothesize that the encoder (*Enc*) and the *Squeeze Layer* (*S*), along with the GRU-based auto-encoder discovers the embedded manifold (\mathcal{M}) in the input space (\mathcal{X}) and learns a mapping to Euclidean space, \mathbb{R}^M . The latent alignment via MMD encourages the network to learn a domain-agnostic manifold which helps us generalize to new domains.

To add further structure to the learned manifold projection (\mathcal{C}), we impose another constraint such that the mapping $\mathcal{C} \rightarrow \mathcal{Y}$ is uniformly continuous¹, i.e. if $x \in \mathcal{C} \rightarrow y \in \mathcal{Y}$ then points in the immediate neighbourhood of x should map to points which are in the immediate neighbourhood of y . Intuitively, we can think of this as a "smoothness" constraint (although it need not be smooth in the mathematical sense). We do this by introducing another loss,

$$\mathcal{L}_{smooth} = \|F(\mathcal{C}) - F(\mathcal{C} + \gamma_{noise} \delta)\|^2 \quad (14)$$

where, $F(\cdot) = R(D(E(\cdot)))$, $\delta \in \mathcal{N}(0, 1)$ is a Gaussian noise vector we use to perturb \mathcal{C} , and γ_{noise} is the scaling factor with which we decide the locality of the perturbation.

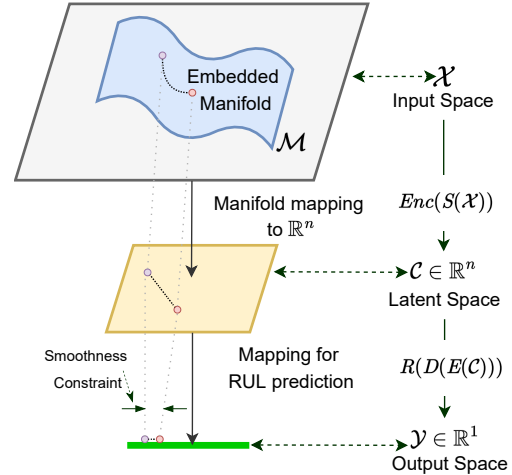


Figure 2: LAMA-Net Architecture: Manifold Perspective

Loss and Optimization

The final loss function of the *LAMA-Net* is:

$$\mathcal{L} = \mathcal{L}_{RUL}^S + \lambda_m \mathcal{L}_{MMD} + \lambda_r \mathcal{L}_{recon}^S + \lambda_r \mathcal{L}_{recon}^T + \lambda_s \mathcal{L}_{smooth}^T + \lambda_s \mathcal{L}_{smooth}^T \quad (15)$$

where, λ_m , λ_r , and λ_s are hyperparameters with which we can control how important each term in the loss function is. The domain adaptation losses only kick in after the first 200 iterations of training.

Since our architecture is end-to-end differentiable, we can easily optimize the loss, \mathcal{L} , using gradient-based methods like gradient descent.

Experiments

In this section, we describe the data set used for the experiments, the experiment procedure and details about the implementation. We also report the comparison of *LAMA-Net* with other state-of-the-art DA techniques. We also provide ablation studies and other investigation to demonstrate the importance of the architecture design decisions.

¹We thank Jan Jitse Venselaar for his help with a bit of math here

C-MAPSS Datasets

To evaluate *LAMA-Net*, we have selected the popular C-MAPSS(Saxena et al. (2008)) benchmark dataset of run-to-failure data of turbofan engines, simulated using a thermodynamic simulation model. The dataset contains information from 21 sensors as well as 3 operating conditions and is composed of four subsets, namely FD001, FD002, FD003 and FD004, which differ in terms of working conditions, fault modes, life spans, and number of engines (Table 3). The operating conditions vary from one in FD001 and FD003, to six in FD002 and FD004. For our experiments, we consider each one of the subsets as source and target domains and perform domain adaptation on all different source-target pairs. Appendix has details about pre-processing.

Experimental Study and Analysis

All experiments used PyTorch (Paszke et al. (2019)) and were run on a single NVIDIA K80/T4 GPU with 2 cores and 12GB of RAM. The batch size was fixed at 128. Initial learning rate was fixed as 1e-3 with a standard Adam optimizer. Exponential Decay with $\gamma = 0.95$, which started the decay after 100 iterations, was used as the learning rate decay for all experiments. We use RMSE and an asymmetric scoring function (Saxena et al. (2008)) as the two metrics to evaluate different models. Details regarding the performance metrics, training procedure, hyperparameter selection and final hyperparameters are present in the Appendix.

Comparison With State-of-the-Art Methods

To evaluate and benchmark *LAMA-Net*, we have chosen to keep the same structure so that the learning capacity of the model remains the same, but compare only the domain adaptation techniques. The autoencoder and the smoothing constraint in *LAMA-Net* are the key aspects of our setup. Therefore, we compare the performance of *LAMA-Net* with other alternatives like DANN (Ganin et al. (2016)), MMD (Gretton et al. (2012))(Tzeng et al. (2014)), CORAL (Sun and Saenko (2016)), and without domain adaptation (No DA) using same DAST architecture with bottlenecks. Table 1 and 2 shows the RMSE and Score for all the source-target combinations using all these modelling alternatives. The standard deviation of Score across the three random seeds are also included in the appendix. Key observations from the results are:

- We can see that *LAMA-Net* is clearly superior to alternatives. Both in RMSE and Score, *LAMA-Net* performs better than the alternatives in a large majority of source-target combinations. And even in cases where *LAMA-Net* is performing slightly worse than an alternative, it makes up for that with increased resilience to random seeds.
- Comparing using the score function makes the superiority even more clearer as the scores of *LAMA-Net* is orders of magnitude better than alternatives, making it the safer choice in any real implementation.
- Even between difficult pairs (FD003-FD002, FD004-FD001, etc) *LAMA-Net* consistently gives better adaptation results. We hypothesize that FD003-FD001 is an easy adaptation task and therefore all the adaptation techniques fail to beat the model which has no adaptation.

Ablation Analysis

In this section, we analyze the contribution and effect of major architectural decisions, such as adding an autoencoder and the smoothness constraint. We are comparing three versions of our proposed model:

- **MMD**: This version just has the MMD based latent alignment
- **MMD + Autoencoder**: This version has the GRU based autoencoder along with the MMD latent Alignment
- **MMD + Autoencoder + Smoothness**: This is the final version, which is what we call *LAMA-Net*.

The RMSE and Score distribution across all source-target combinations is depicted in Figure 3. We can see that adding the Autoencoder brings with it the maximum benefit as there is a large shift in means and reduction in variation between **MMD** and **MMD + Autoencoder**, in both RMSE and Score. The addition of the smoothness constraint also brings, but notably smaller, improvement in RMSE and Score.

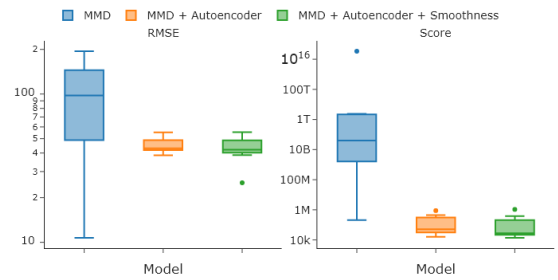


Figure 3: RMSE and Score of different versions of the proposed model

To further investigate and validate our claims of manifold learning, we used t-SNE(van der Maaten and Hinton (2008)) to visualize the bottleneck layer (\mathcal{C}) and the linear projection layer (\mathcal{O}) (Figure 4) using the training data. We have also color-coded the different points using the RUL labels.

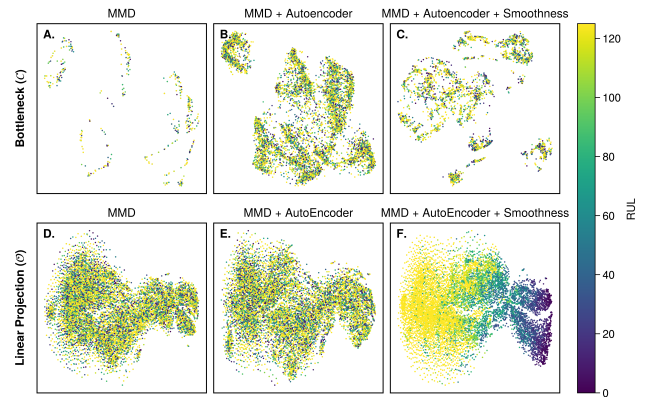


Figure 4: t-SNE Visualization of \mathcal{C} and \mathcal{O} for different versions of the proposed model

Table 1: Average RMSE with S.D for RUL Prediction across all source-target combinations (3 Random seeds)

Source	Target	No DA	DANN	MMD	CORAL	LAMA-Net
FD001	FD002	96.04±1.96	97.92±25.65	100.31±11.2	105.11±10.42	53.88±0.01
FD001	FD003	50.04±3.7	44.62±4.5	45.57±8.73	35.76±8.88	40.54±1.24
FD001	FD004	110.38±4.93	101.51±19.18	51.43±45.22	94.28±9.27	55.26±0.08
FD002	FD001	103.26±19.79	128.13±27.55	118.25±17.64	122.43±37.47	41.87±0.21
FD002	FD003	104.79±8.39	95.68±16.99	112.11±11.93	123.04±41.84	41.9±0.4
FD002	FD004	75.45±25.7	75.9±24.42	75.3±25.44	74.98±18.74	35.61±7.53
FD003	FD001	27.9±5.53	63.27±4.99	47.03±10.15	70.25±54.09	41.01±11.89
FD003	FD002	103.12±9.98	109.56±13.96	104±16.34	100.3±31.2	57.05±3.75
FD003	FD004	78.81±35.47	84.02±26.42	99.73±14.99	154.39±52.68	50.89±8.52
FD004	FD001	116.19±36.27	165.96±18.02	181.52±9.2	118.59±22.01	42.78±0.37
FD004	FD002	46.32±16.01	60.79±8.81	80.47±6.41	83.46±7.86	34.8±0.37
FD004	FD003	100.35±24.6	129.71±59.84	153.38±23.24	108.62±56.18	42.76±0.52

Table 2: Average Score for RUL Prediction across all source-target combinations (3 Random seeds)

Source	Target	No DA	DANN	MMD	CORAL	LAMA-Net
FD001	FD002	9.25E+18	1.65E+11	8.56E+11	1.48E+17	9.23E+05
FD001	FD003	2.83E+05	1.35E+06	3.77E+05	1.11E+06	2.24E+04
FD001	FD004	5.61E+21	3.64E+10	4.97E+10	4.16E+14	9.99E+05
FD002	FD001	9.72E+09	3.41E+17	1.15E+16	1.48E+16	2.07E+04
FD002	FD003	2.31E+08	1.16E+13	1.89E+16	2.29E+18	2.30E+04
FD002	FD004	6.74E+28	2.69E+27	5.13E+27	3.12E+26	1.51E+05
FD003	FD001	1.33E+04	2.04E+10	8.31E+07	1.46E+09	1.51E+05
FD003	FD002	7.87E+18	5.06E+10	2.46E+10	8.52E+17	8.62E+06
FD003	FD004	8.06E+19	3.32E+10	9.27E+09	1.93E+17	5.90E+06
FD004	FD001	1.12E+10	7.57E+10	6.76E+11	3.31E+14	3.17E+04
FD004	FD002	4.21E+23	2.55E+21	2.17E+25	1.23E+30	6.14E+04
FD004	FD003	3.61E+09	2.38E+11	8.31E+11	6.84E+12	3.14E+04

We can see that adding the autoencoder to reconstruct the input (\mathcal{X}) from the bottleneck (\mathcal{C}) immediately adds a lot of structure to the representation (Fig 4: B). We hypothesize that this structure that the model is capturing is a domain agnostic manifold in the input space and is helping it generalize across domains. We also note that the smoothness constraint, whose main purpose is to act on the linear projection (\mathcal{O}), has also an upstream effect on the learned manifold. \mathcal{C} seems to be more sparse and separated with local clustering of similar colored points.

The linear projection (\mathcal{O}) layer is hardly affected by the addition of the autoencoder (Fig 4: D and E). The smoothness constraint doesn't change the overall shape of the manifold, but it rearranges the points in a way that is amenable to final prediction. We can observe a smooth transition from the healthy datapoints on the left to the ones that is at failure (on the right). And we hypothesize that this re-arrangement also helps the model generalize across domains and avoids highly unstable prediction functions.

Conclusion

In this paper, we develop a novel deep learning architecture (*LAMA-Net*) for Unsupervised Domain Adaptation (UDA)

by learning a domain invariant manifold via a combination of losses - regular MSE loss for RUL prediction, MMD loss for aligning the latent representations across source and target domains, reconstruction loss from an autoencoder to enable manifold learning, and a smoothness constraint which enforces uniform continuity in the function that maps the learned manifold to the output space. We then evaluate this architecture on the popular run-to-failure C-MAPSS dataset for turbofan engines and compare against other state-of-the-art alternatives like MMD, CORAL, and DANN. Using RMSE and a asymmetric scoring function, we show that the proposed approach is superior to alternatives in both from the RMSE or Score as well as stability to random seeds perspective. By further analysis into the major architecture decisions, we show how adding an autoencoder enables manifold learning and thereby improves the generalization capability by a large margin. And further the smoothness constraint manage to rearrange the linear projection in a way that makes the final linear layer to predict the RUL with relative ease and stability. We have made available the code at <https://github.com/repo> under MIT License.

References

- Ajakan, H.; Germain, P.; Larochelle, H.; Laviolette, F.; and Marchand, M. 2014. Domain-adversarial neural networks. *arXiv preprint arXiv:1412.4446*.
- Baktash, M.; Harandi, M. T.; Lovell, B. C.; and Salzmann, M. 2014. Domain Adaptation on the Statistical Manifold. *2014 IEEE Conference on Computer Vision and Pattern Recognition*, 2481–2488.
- Ben-David, S.; Blitzer, J.; Crammer, K.; Kulesza, A.; Pereira, F.; and Vaughan, J. W. 2010. A theory of learning from different domains. *Machine Learning*, 79(1): 151–175.
- Borgwardt, K. M.; Gretton, A.; Rasch, M. J.; Kriegel, H.-P.; Schölkopf, B.; and Smola, A. J. 2006. Integrating structured biological data by Kernel Maximum Mean Discrepancy. *Bioinformatics*, 22(14): e49–e57.
- Breiman, L. 2001. Random Forests. *Machine Learning*, 45(1): 5–32.
- Cayton, L. 2005. Algorithms for manifold learning. Technical report.
- Chen, T.; and Guestrin, C. 2016. XGBoost: A Scalable Tree Boosting System. In *Proceedings of the 22nd ACM SIGKDD International Conference on Knowledge Discovery and Data Mining*, KDD '16, 785–794. New York, NY, USA: Association for Computing Machinery. ISBN 9781450342322.
- Cho, K.; van Merriënboer, B.; Gülçehre, Ç.; Bahdanau, D.; Bougares, F.; Schwenk, H.; and Bengio, Y. 2014. Learning Phrase Representations using RNN Encoder-Decoder for Statistical Machine Translation. In Moschitti, A.; Pang, B.; and Daelemans, W., eds., *Proceedings of the 2014 Conference on Empirical Methods in Natural Language Processing, EMNLP 2014, October 25-29, 2014, Doha, Qatar, A meeting of SIGDAT, a Special Interest Group of the ACL*, 1724–1734. ACL.
- Cubillo, A.; Perinpanayagam, S.; and Esperon-Miguez, M. 2016. A review of physics-based models in prognostics: Application to gears and bearings of rotating machinery. *Advances in Mechanical Engineering*, 8(8): 1687814016664660.
- de Oliveira da Costa, P. R.; Akçay, A.; Zhang, Y.; and Kaymak, U. 2020. Remaining useful lifetime prediction via deep domain adaptation. *Reliability Engineering & System Safety*, 195: 106682.
- Deng, J.; Zhang, Z.; Eyben, F.; and Schuller, B. 2014. Autoencoder-based Unsupervised Domain Adaptation for Speech Emotion Recognition. *IEEE Signal Processing Letters*, 21: 1068–1072.
- Ding, Y.; Jia, M.; and Cao, Y. 2021. Remaining Useful Life Estimation Under Multiple Operating Conditions via Deep Subdomain Adaptation. *IEEE Transactions on Instrumentation and Measurement*, 70: 1–11.
- Drucker, H.; Burges, C.; Kaufman, L.; Smola, A.; and Vapnik, V. 1997. Support vector regression machines. *Adv Neural Inform Process Syst*, 28: 779–784.
- Fang, X.; Lin, S.; Huang, X.; Lin, F.; Yang, Z.; and Igarashi, S. 2018. A review of data-driven prognostic for IGBT remaining useful life. *Chinese Journal of Electrical Engineering*, 4(3): 73–79.
- Fernando, B.; Habrard, A.; Sebban, M.; and Tuytelaars, T. 2013. Unsupervised Visual Domain Adaptation Using Subspace Alignment. In *2013 IEEE International Conference on Computer Vision*, 2960–2967.
- Ganin, Y.; Ustinova, E.; Ajakan, H.; Germain, P.; Larochelle, H.; Laviolette, F.; Marchand, M.; and Lempitsky, V. 2016. Domain-adversarial training of neural networks. *The journal of machine learning research*, 17(1): 2096–2030.
- Gretton, A.; Borgwardt, K. M.; Rasch, M. J.; Schölkopf, B.; and Smola, A. 2012. A Kernel Two-Sample Test. *J. Mach. Learn. Res.*, 13(null): 723–773.
- Heimes, F. O. 2008. Recurrent neural networks for remaining useful life estimation. In *2008 International Conference on Prognostics and Health Management*, 1–6.
- Hochreiter, S.; and Schmidhuber, J. 1997. Long Short-Term Memory. *Neural Computation*, 9: 1735–1780.
- Hsu, C.-S.; and Jiang, J.-R. 2018. Remaining useful life estimation using long short-term memory deep learning. In *2018 IEEE International Conference on Applied System Invention (ICASI)*, 58–61.
- Huang, J.; Gretton, A.; Borgwardt, K.; Schölkopf, B.; and Smola, A. 2006. Correcting Sample Selection Bias by Unlabeled Data. In Schölkopf, B.; Platt, J.; and Hoffman, T., eds., *Advances in Neural Information Processing Systems*, volume 19. MIT Press.
- Huang, R.; Xi, L.; Li, X.; Richard Liu, C.; Qiu, H.; and Lee, J. 2007. Residual life predictions for ball bearings based on self-organizing map and back propagation neural network methods. *Mechanical Systems and Signal Processing*, 21(1): 193–207.
- Jianzhong, S.; Hongfu, Z.; Haibin, Y.; and Pecht, M. 2010. Study of ensemble learning-based fusion prognostics. In *2010 Prognostics and System Health Management Conference*, 1–7.
- Lei, Y.; Li, N.; Guo, L.; Li, N.; Yan, T.; and Lin, J. 2018. Machinery health prognostics: A systematic review from data acquisition to RUL prediction. *Mechanical Systems and Signal Processing*, 104: 799–834.
- Li, F.; Zhang, L.; Chen, B.; Gao, D.; Cheng, Y.; Zhang, X.; Yang, Y.; Gao, K.; Huang, Z.; and Peng, J. 2018a. A Light Gradient Boosting Machine for Remaining Useful Life Estimation of Aircraft Engines. In *2018 21st International Conference on Intelligent Transportation Systems (ITSC)*, 3562–3567.
- Li, J.; Li, X.; and He, D. 2019. Domain Adaptation Remaining Useful Life Prediction Method Based on AdaBN-DCNN. In *2019 Prognostics and System Health Management Conference (PHM-Qingdao)*, 1–6.
- Li, X.; Ding, Q.; and Sun, J.-Q. 2018. Remaining useful life estimation in prognostics using deep convolution neural networks. *Reliability Engineering & System Safety*, 172: 1–11.
- Li, Y.; Wang, N.; Shi, J.; Hou, X.; and Liu, J. 2018b. Adaptive Batch Normalization for practical domain adaptation. *Pattern Recognition*, 80: 109–117.
- Long, M.; Cao, Y.; Wang, J.; and Jordan, M. I. 2015. Learning Transferable Features with Deep Adaptation Networks. In Bach, F. R.; and Blei, D. M., eds., *Proceedings of the 32nd International Conference on Machine Learning, ICML 2015, Lille, France, 6-11 July 2015*, volume 37 of *JMLR Workshop and Conference Proceedings*, 97–105. JMLR.org.
- Ma, Z.; Guo, J.; Mao, S.; and Gu, T. 2020. An interpretability research of the Xgboost algorithm in remaining useful life prediction. In *2020 International Conference on Big Data & Artificial Intelligence & Software Engineering (ICBASE)*, 433–438.
- Muneer, A.; Mohd Taib, S.; Fati, S.; and Alhussian, H. 2021. Deep-Learning Based Prognosis Approach for Remaining Useful Life Prediction of Turbofan Engine. *Symmetry*, 13: 1861.
- Paszke, A.; Gross, S.; Massa, F.; Lerer, A.; Bradbury, J.; Chanan, G.; Killeen, T.; Lin, Z.; Gimelshein, N.; Antiga, L.; Desmaison, A.; Kopf, A.; Yang, E.; DeVito, Z.; Raison, M.; Tejani, A.; Chilamkurthy, S.; Steiner, B.; Fang, L.; Bai, J.; and Chintala, S. 2019. PyTorch: An Imperative Style, High-Performance Deep Learning Library. In Wallach, H.; Larochelle, H.; Beygelzimer, A.; d'Alché-Buc, F.; Fox, E.; and Garnett, R., eds., *Advances in Neural Information Processing Systems 32*, 8024–8035. Curran Associates, Inc.

- Peng, C.; Chen, Y.; Chen, Q.; Tang, Z.; Li, L.; and Gui, W. 2021a. A Remaining Useful Life Prognosis of Turbofan Engine Using Temporal and Spatial Feature Fusion. *Sensors*, 21: 418.
- Peng, C.; Chen, Y.; Chen, Q.; Tang, Z.; Li, L.; and Gui, W. 2021b. A Remaining Useful Life Prognosis of Turbofan Engine Using Temporal and Spatial Feature Fusion. *Sensors*, 21(2).
- Ragab, M.; Chen, Z.; Wu, M.; Foo, C. S.; Kwok, C. K.; Yan, R.; and Li, X. 2021. Contrastive Adversarial Domain Adaptation for Machine Remaining Useful Life Prediction. *IEEE Transactions on Industrial Informatics*, 17(8): 5239–5249.
- Saxena, A.; Goebel, K.; Simon, D.; and Eklund, N. H. W. 2008. Damage propagation modeling for aircraft engine run-to-failure simulation. *2008 International Conference on Prognostics and Health Management*, 1–9.
- Si, X.-S.; Wang, W.; Hu, C.-H.; and Zhou, D.-H. 2011. Remaining useful life estimation—a review on the statistical data driven approaches. *European journal of operational research*, 213(1): 1–14.
- Sriperumbudur, B. K.; Gretton, A.; Fukumizu, K.; Schölkopf, B.; and Lanckriet, G. R. G. 2010. Hilbert Space Embeddings and Metrics on Probability Measures. *J. Mach. Learn. Res.*, 11: 1517–1561.
- Sun, B.; and Saenko, K. 2016. Deep CORAL: Correlation Alignment for Deep Domain Adaptation.
- Tzeng, E.; Hoffman, J.; Zhang, N.; Saenko, K.; and Darrell, T. 2014. Deep Domain Confusion: Maximizing for Domain Invariance. *cvpr 2014*.
- van der Maaten, L.; and Hinton, G. 2008. Visualizing Data using t-SNE. *Journal of Machine Learning Research*, 9(86): 2579–2605.
- Vaswani, A.; Shazeer, N.; Parmar, N.; Uszkoreit, J.; Jones, L.; Gomez, A. N.; Kaiser, L. u.; and Polosukhin, I. 2017. Attention is All you Need. In Guyon, I.; Luxburg, U. V.; Bengio, S.; Wallach, H.; Fergus, R.; Vishwanathan, S.; and Garnett, R., eds., *Advances in Neural Information Processing Systems*, volume 30. Curran Associates, Inc.
- Wang, J.; Feng, W.; Chen, Y.; Yu, H.; Huang, M.; and Yu, P. S. 2018. Visual Domain Adaptation with Manifold Embedded Distribution Alignment. *Proceedings of the 26th ACM international conference on Multimedia*.
- Wang, Y.; Zhao, Y.; and Addepalli, S. 2020. Remaining Useful Life Prediction using Deep Learning Approaches: A Review. *Procedia Manufacturing*, 49: 81–88. Proceedings of the 8th International Conference on Through-Life Engineering Services – TESConf 2019.
- Wei, C.; Luo, S.; Ma, X.; Ren, H.; Zhang, J.; and Pan, L. 2016. Locally embedding autoencoders: a semi-supervised manifold learning approach of document representation. *PLoS one*, 11(1): e0146672.
- Wu, H.; Xu, J.; Wang, J.; and Long, M. 2021. Autoformer: Decomposition Transformers with Auto-Correlation for Long-Term Series Forecasting. In Ranzato, M.; Beygelzimer, A.; Dauphin, Y. N.; Liang, P.; and Vaughan, J. W., eds., *Advances in Neural Information Processing Systems 34: Annual Conference on Neural Information Processing Systems 2021, NeurIPS 2021, December 6-14, 2021, virtual*, 22419–22430.
- Zhang, A.; Wang, H.; Li, S.; Cui, Y.; Liu, Z.; Guanci, Y.; and Hu, J. 2018. Transfer Learning with Deep Recurrent Neural Networks for Remaining Useful Life Estimation. *Applied Sciences*, 8: 2416.
- Zhang, Z.; Song, W.; and Li, Q. 2021. Dual Aspect Self-Attention based on Transformer for Remaining Useful Life Prediction. *IEEE transactions on instrumentation and measurement*.
- Zheng, S.; Ristovski, K.; Farahat, A.; and Gupta, C. 2017. Long Short-Term Memory Network for Remaining Useful Life estimation. In *2017 IEEE International Conference on Prognostics and Health Management (ICPHM)*, 88–95.
- Zhou, H.; Zhang, S.; Peng, J.; Zhang, S.; Li, J.; Xiong, H.; and Zhang, W. 2021. Informer: Beyond Efficient Transformer for Long Sequence Time-Series Forecasting. In *Thirty-Fifth AAAI Conference on Artificial Intelligence, AAAI 2021, Thirty-Third Conference on Innovative Applications of Artificial Intelligence, IAAI 2021, The Eleventh Symposium on Educational Advances in Artificial Intelligence, EAAI 2021, Virtual Event, February 2-9, 2021*, 11106–11115. AAAI Press.

Appendix

Datasets - Detailed

The popular C-MAPSS(Saxena et al. (2008)) benchmark dataset of run-to-failure data of turbofan engines, simulated using a thermo-dynamic simulation model. The dataset contains information from 21 sensors as well as 3 operating conditions and is composed of four subsets, namely FD001, FD002, FD003 and FD004, which differ in terms of working conditions, fault modes, life spans, and number of engines (Table 3).

Each subset is further divided into a training set and a testing set. Data sets consists of multiple multivariate time series. Each data set is further divided into training and test subsets. Each time series begins with the engine running normally, and at some point during the series, a defect appears. The fault increases in size in the training set till system failure. The time series in the test set finishes before the system fails. The goal of the competition is to forecast how many operational cycles will remain in the test set before failure, or how many operational cycles will remain in the engine after the final cycle. A vector of accurate Remaining Useful Life (RUL) values for the test data is also provided.

The properties of this dataset regarding the demonstration of prognostic approaches are as follows.

- This is a simulated dataset acquired from commercial software instead of real turbofan engines. Although the degradation processes are simulated as realistic as possible with the consideration of many variability sources, they are still different from real cases.
- This dataset contains 21 observations which are composed of different types of features, such as the temperature, pressure, speed, and bleed. Therefore, it is a typical prognostic issue of multi-sensor information fusion.
- This dataset includes six different operational conditions. The time-varying operational conditions cause fluctuation of the degradation trends. Thus, it is suitable for the study of domain adaptation between time-varying operational conditions and degradation trends.

Data Preprocessing

The temporal dataset had information coming in from 21 sensors and 3 operational settings. Although we note that 7 sensor values have constant readings in FD001 and FD003, we have still kept all 21 sensor readings and let the model figure out which sensors holds information necessary for prediction. In order to adapt for different sequence lengths, increase the number of observations the model is trained on, and allow information from past multivariate temporal sequences influence the RUL prediction at any point in time, we employed a sliding window with stride set to one for feature generation. Let the size of the window be T_w , then each window in a sequence, $\mathbf{x} = (x_t)_{t=0}^T$, is defined as $\mathcal{W}_t = \{x_{t-T_w}, \dots, x_{t-1}\}$. For training the model, the RUL corresponding to the window (RUL_t) is equal to the RUL at time t . No additional feature engineering is done on the input data.

We further normalize the input data by scaling each feature individually such that it is in the (0,1) range using the min-max normalization method

$$norm(x_t^{i,j}) = \frac{x_t^{i,j} - \min(x^j)}{\max(x^j) - \min(x^j)} \quad (16)$$

where, $x_t^{i,j}$ is the original i -th datapoint of the j -th input feature at time t and x^j is the vector of all inputs of the j -th input feature.

A typical run-to-failure dataset will have the sensor readings, starting when the machine is in good health, and ending when the machine fails. The RUL labels is something we need to derive from the run-to-failure dataset. For a sequence length of T , a naive approach is to assume a linear decay and set RUL at any time t , as remaining time on the run-to-failure data ($R_t = T - t$). But Heimes (2008) has shown that it is a reasonable assumption to estimate RUL as a constant value when the engines operate in good health. Similar to other works (Hsu and Jiang (2018), Peng et al. (2021b)) in the area using the dataset, we propose to use a piece-wise linear degradation model to define RUL where the initial period of a run-to-failure data is mapped to a constant RUL value (R_c) and then switch to a linear degradation based on time.

$$RUL_t = \min(T - t, R_c) \quad (17)$$

We have chosen R_c to be 125 as suggested by other works using the same dataset. In addition to this we have also scaled the RUL to lie in the range (0,1), by dividing the RUL with maximum value of RUL (which is R_c).

$$scale(RUL_t) = \frac{RUL_t}{R_c} \quad (18)$$

Performance Metrics

In line with other work using this dataset, the performance of the models was evaluated using the Root Mean Squared Error (RMSE) and an asymmetric scoring function (Saxena et al. (2008)).

$$Score = \begin{cases} \sum_{i=1}^n e^{-(E_i/10)} - 1 & \text{for } E_i < 0; \\ \sum_{i=1}^n e^{(E_i/13)} - 1 & \text{for } E_i \geq 0 \end{cases} \quad (19)$$

where n is the number of engines, $E_i = \hat{RUL}_i - RUL_i$

Scoring function is structurally an asymmetric function (Figure 5) that penalises positive errors more than negative errors. RMSE considers an error on either side equally serious, but in RUL prediction, predicting a longer RUL than actual is a much more serious problem than predicting shorter than actual. The scoring function takes care of this nuance in evaluation.

Training Procedure

We choose one of the four C-MAPSS datasets as the source dataset and use our proposed method to learn the RUL on all the other three datasets, without using the RUL labels on those. We use the official training and test split for our validation, and we do create a validation set from the training data using random split with the seed 42. The validation data

Table 3: Dataset Summary

	FD001	FD002	FD003	FD004
Train trajectories	100	260	100	248
Test trajectories	100	259	100	249
Conditions	1 (Sea level)	6	1 (Sea level)	6
Fault Modes (Degradation)	1 (HPC)	1 (HPC)	2 (HPC and Fan)	2 (HPC and Fan)
Max/min cycles in train set	362/128	378/128	25/145	543/128
Max/min cycles in test set	303/31	367/21	475/38	486/19
Train samples	17731	48558	21220	56815
Test samples	100	259	100	248

Table 4: Selected Hyperparameters

Hyperparameter	Ours	DANN	MMD	CORAL
<i>Window</i>	40	40	40	40
<i>Epochs</i>	40	40	40	40
<i>Batch Size</i>	128	128	128	128
<i>DAST: Attention Dimension</i>	32	32	32	32
<i>DAST: # of Encoder Layers</i>	3	3	3	3
<i>DAST: # of Decoder Layers</i>	1	1	1	1
<i>DAST: # of attention heads</i>	4	4	4	4
<i>Squeeze Layer</i>	500-200	500-200	500-200	500-200
<i>Expand Layer</i>	200-500	200-500	200-500	200-500
<i>AutoEncoder</i>	GRU(hidden_size=1, num_layers=1)	NA	NA	NA
<i>Discrepancy Weight (λ_m)</i>	0.35	NA	0.2	0.2
<i>DANN Weight</i>	NA	0.2	NA	NA
<i>Reconstruction Weight (λ_{recon})</i>	0.2	NA	NA	NA
<i>Smoothness Weight (λ_{smooth})</i>	0.35	NA	NA	NA
<i>Local Perturbation (γ_{noise})</i>	0.1	NA	NA	NA

Table 5: Standard Deviation of Score

Source	Target	No DA	DANN	MMD	CORAL	LAMA-Net
FD001	FD002	1.31E+19	1.73E+11	1.19E+12	2.09E+17	1.82E+04
FD001	FD003	1.48E+05	2.50E+05	3.28E+05	1.28E+06	5.59E+03
FD001	FD004	7.93E+21	4.06E+10	2.79E+10	5.88E+14	4.61E+04
FD002	FD001	7.67E+09	4.83E+17	1.60E+16	2.08E+16	3.27E+03
FD002	FD003	1.55E+08	1.65E+13	2.67E+16	3.24E+18	3.65E+03
FD002	FD004	9.53E+28	3.81E+27	7.25E+27	4.42E+26	1.04E+05
FD003	FD001	8.40E+03	2.68E+10	1.07E+08	2.07E+09	1.84E+05
FD003	FD002	1.11E+19	5.55E+10	3.20E+10	1.21E+18	1.16E+07
FD003	FD004	1.13E+20	4.68E+10	8.46E+09	2.73E+17	7.89E+06
FD004	FD001	1.58E+10	6.85E+10	8.57E+11	4.69E+14	4.20E+03
FD004	FD002	5.95E+23	3.61E+21	2.16E+25	1.74E+30	4.54E+03
FD004	FD003	4.84E+09	2.10E+11	1.11E+12	9.67E+12	5.29E+03

is only used for monitoring the learning as we do not use any early stopping while training the model. We use mini-batch Gradient Descent for training the model and we randomly select equal number of samples from source and target to form a mini-batch. In all our experiments, we ran the training for 40 epochs with a learning rate decay. We have repeated all experiments using 3 different random seeds (1, 123074,

and 2457) and reported the mean and standard deviation to assess the performance as well as stability of the modelling alternatives.

Hyperparameter Selection

For all our experiments, we have chosen the same DAST model with the Squeeze and Expand Layers to maintain con-

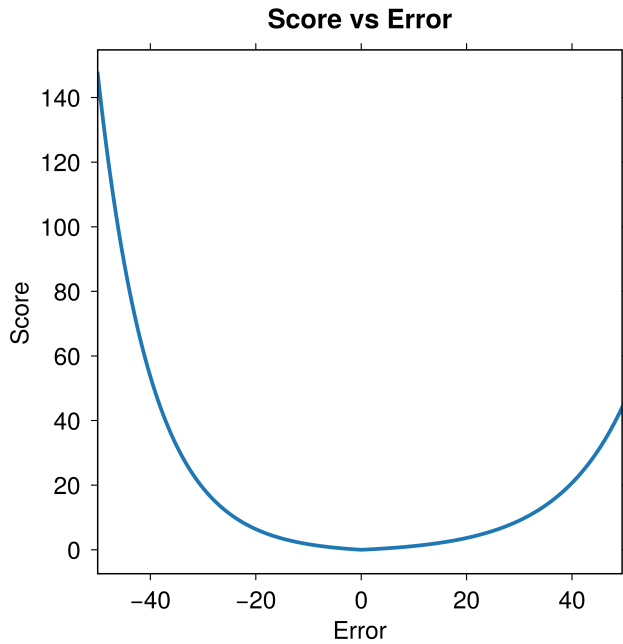


Figure 5: Asymmetric Nature of the Score Metric

sistency in comparison with other techniques. The key hyperparameters for the DAST model are: *hidden size for the attention* = 32, *number of encoder layers* = 3, *number of decoder layers* = 1 and *number of heads for the attention mechanism* = 4. The *Squeeze Layer* is a multi-layered feed forward network with 500 and 200 units, and the *Expand Layer* is just the opposite with 200 and 500 units such that the output from the *Expand Layer* has the same dimensions as the input to the *Squeeze Layer*. This initial set of *fixed hyperparameters* are fixed such that we have enough capacity in the models to learn the required patterns. Given the structure of the network, we focus our hyperparameter tuning on the core DA mechanism with the below grid:

- $\lambda_m, \lambda_r, \text{ and } \lambda_s \rightarrow [0.1, 0.2, 0.35, 0.5]$
- $\gamma_{noise} \rightarrow [0.1, 0.01]$
- Autoencoder $\rightarrow [”GRU”, ”LSTM”, ”RNN”]$

Instead of selecting a configuration for each source-target combinations, we chose a set of hyperparameters which performed better on the validation source RUL across all the source-target combinations. This helps us come up with a set of hyperparameters which has more generalization capabilities.

Final Hyperparameters

The final set of hyperparameters used in the experiments are in Table 4.

Additional Results

The standard deviation across three runs with different random seeds for the Score is in Table 5.